HHS Public Access

Author manuscript

Nat Neurosci. Author manuscript; available in PMC 2012 February 06.

Published in final edited form as:

Nat Neurosci. ; 14(8): 1001–1008. doi:10.1038/nn.2866.

Loss of Activity-Induced Phosphorylation of MeCP2 Enhances Synaptogenesis, LTP, and Spatial Memory

Hongda Li[1,2], **Xiaofen Zhong**[2], **Kevin Fongching Chau**[2], **Emily Cunningham Williams**[1,2], and **Qiang Chang**[1,2,3,*]

[1]Genetics Training Program, University of Wisconsin-Madison, 1500 Highland Avenue, Madison, WI 53705, USA

[2]Waisman Center, University of Wisconsin-Madison, 1500 Highland Avenue, Madison, WI 53705, USA

[3]Department of Genetics and Neurology, University of Wisconsin-Madison, 1500 Highland Avenue, Madison, WI 53705, USA

Abstract

DNA methylation-dependent epigenetic mechanisms underlie the development and function of the mammalian brain. MeCP2 expresses highly in neurons, and functions as a molecular linker between DNA methylation, chromatin remodeling and transcription regulation. Previous *in vitro* studies showed neuronal activity-induced phosphorylation (NAIP) of MeCP2 precedes its release from the *Bdnf* promoter and the ensuing *Bdnf* transcription. However, the *in vivo* function of this phosphorylation event remains elusive. We generated knockin mice that lack NAIP of MeCP2, and show here the *Mecp2* phospho-mutant mice perform better in hippocampus-dependent memory tests, present enhanced LTP at two synapses in the hippocampus, and show increased excitatory synaptogenesis. At the molecular level, the phospho-mutant MeCP2 protein binds more tightly to several MeCP2 target gene promoters and alters the expression of these genes. Our results supply the first genetic evidence that NAIP of MeCP2 is required in modulating dynamic functions of the adult mouse brain.

The genetic and epigenetic mechanisms underlying the development, maintenance, and function of the mammalian nervous system have been extensively studied over the years. To understand what functional role DNA methylation-dependent epigenetic mechanisms may play in any of these biological processes, it is important to study how DNA methylation and

*Correspondence should be addressed to Q.C. (qchang@waisman.wisc.edu).

Author Contributions

Q.C. directed the studies. H.L., X.Z., and Q.C. conceived and designed the experiments. H.L. performed the Western blot, mouse behavioral tests, chromatin immunoprecipitation experiments, gene expression studies, imaging and image analysis. K.F.C. performed mouse behavioral tests. X.Z. performed all electrophysiology experiments, neuronal culture and hippocampal slice experiments, and immunostaining. E.C.W. performed immunostaining. The paper was written by Q.C., H.L., and X.Z. and commented on by all authors.

Competing financial interests

The authors declare no competing financial interests.

the recognition of DNA methylation by the methyl-DNA binding domain containing proteins (MBDs) may be dynamically regulated in neuronal nuclei in response to extracellular signals. While there is pharmacological[1,2] and genetic[3] evidence that dynamic DNA methylation is required for learning and memory, relatively little is known about how binding to methylated DNA by the MBDs may be dynamically regulated to support normal brain functions.

As the founding member of the MBD gene family, *Mecp2* (methyl-CpG binding protein 2) encodes a protein that specifically binds to methylated DNA and represses transcription[4,5]. Earlier studies show that MeCP2 interacts with the transcriptional repressor mSin3A and histone deacetylases[6], suggesting it may function as a molecular linker between DNA methylation, chromatin remodeling and subsequent gene silencing[7]. However, recent studies also demonstrate that MeCP2 may activate transcription of some genes, while repress transcription of others[8,9]. Mutations in the X-linked human *MECP2* gene cause Rett syndrome (RTT)[10–13], an autism spectrum neurodevelopmental disorder that predominantly affects females[14,15]. At an estimated prevalence of 1 in 10,000–15,000 girls, RTT is the second most common X-linked mental retardation in females.

To better understand the functions of MeCP2 and help reveal the molecular mechanism of RTT, it is important to study how MeCP2 dynamically regulates neuronal gene transcription in response to diverse extracellular stimuli, and to reveal the physiological significance of such regulation. The most common extracellular stimulus in the brain is neuronal activity. Two earlier *in vitro* studies in rat neurons have shown that neuronal activity-induced phosphorylation (NAIP) at serine 421 (S421) precedes the release of MeCP2 from the neuronal specific promoter of the brain-derived neurotrophic factor (*Bdnf*) gene and the subsequent expression of BDNF[16,17]. Recently, a more detailed analysis of the mouse brain by mass spectrometry has identified NAIP at two serines, S421 and S424 of the MeCP2 protein[18]. Moreover, both sensory inputs and psychostimulants have been shown to induce phosphorylation of MeCP2 at S421 in the intact mouse brain[17,19]. Collectively, these studies raise the possibility that NAIP of MeCP2 may serve as a molecular switch on the chromatin for dynamically modulating neuronal functions. To reveal what *in vivo* function requires NAIP of MeCP2, we have generated knockin mice that carry point mutations in the endogenous *Mecp2* gene locus to abolish phosphorylation at both S421 and S424. We show here that phosphorylation at S421 can be induced by depolarization, high frequency electrical stimulation, and behavioral training in the hippocampus of wild type mice; and that the $Mecp2^{S421A;S424A/y}$ mice lack phosphorylation at S421 in the brain at both the baseline level and after seizure. We further demonstrate that the $Mecp2^{S421A;S424A/y}$ mice perform better in two hippocampus-dependent learning and memory tests than their wild type littermates, present enhanced long-term potentiation at both the Schaffer collateral-CA1 synapses and the mossy fiber-CA3 synapses, have increased excitatory synaptogenesis, and show corresponding gene expression changes that are consistent with these phenotypes. Finally, to take advantage of the consistency of the anti-flag antibody so that we may better quantify the promoter occupancy of the phospho-mutant MeCP2 protein, we generated two novel *Mecp2* knockin alleles: the $Mecp2^{S421A;S424A\text{-}flag/y}$ mice expressing the $MeCP2^{S421A;S424A}$-flag protein from the endogenous *Mecp2* locus and the $Mecp2^{WT\text{-}flag/y}$

mice expressing the MeCP2-flag protein from the endogenous *Mecp2* locus. We show that the MeCP2$^{S421A;S424A}$-flag protein binds more tightly to known MeCP2 target gene promoters than does the MeCP2-flag protein, indicating the phospho-dead form of MeCP2 may function as a hypermorph. Our findings provide the first genetic evidence that neuronal activity-induced MeCP2 phosphorylation is required for the development, maintenance, and function of the adult mouse brain. These results may be relevant for understanding RTT disease mechanisms. Moreover, these results add to the emerging picture of epigenetic regulation of nervous system function, which include not only changes in DNA methylation itself, but also a critical role for stimulus-dependent phosphorylation of a methyl-DNA binding protein.

RESULTS

Loss of NAIP of MeCP2 in *Mecp2*$^{S421A;S424A/y}$ mice

To compare the level of S421 phosphorylation in the silent hippocampus with that in the active hippocampus, we treated freshly prepared hippocampal slices with either tetradotoxin (TTX, to suppress neuronal activity) or potassium chloride (KCl, to depolarize neurons), and performed double immunostaining with a phospho-S421 (p-S421) specific antibody and a NeuN antibody (a neuronal marker). The intensity of p-S421 signal was dramatically higher in the KCl-treated slices than in the TTX-treated slices (Fig. 1a,e), indicating the induction of S421 phosphorylation by depolarization. As a control, the intensity of NeuN signal was the same in KCl- and TTX-treated slices (Fig. 1a). We next tested whether phosphorylation of S421 may be induced by more physiologically relevant stimuli. High frequency electrical stimulation (HFS) is commonly used to induce long-term potentiation (LTP) in hippocampal slices. Using the same p-S421 specific antibody, we detected more than 100% increase in the intensity of p-S421 signal after HFS in acute hippocampal slices, as compared to its level in slices under baseline electrical stimulation (Fig. 1b,e). Again NeuN immunoreactivity was similar in slices receiving either baseline stimulation or HFS (Fig. 1b). Finally, we tested whether phosphorylation of S421 may be induced by behavioral trainings, such as contextual fear conditioning and Morris water maze. In the contextual fear training experiment, we compared p-S421 immunoreactivity in hippocampal sections from mice that received shock immediately after being put into the box (immediate shock control) and mice that received shock two minutes after being put into the box (context trained), and found a 59% increase of p-S421 signal in the context trained mice over the immediate shock control (Fig. 1c,e). In the Morris water maze training experiment, we compared p-S421 immunoreactivity in hippocampal sections from mice that received the hidden platform version of Morris water maze (WM) training (WM trained) and mice that swam the same amount of time in the same tank with no platform (yoked/swimming control), and found a 88% increase of p-S421 signal in the hippocampus of WM trained mice over the yoked/swimming control (Fig. 1d,e). In addition to co-staining with NeuN (Fig. 1c,d), we performed immunostaining against total MeCP2 on the adjacent sections, and detected no difference in total MeCP2 expression between the context trained group and the immediate shock control, and between the WM trained group and the yoked/swimming control (Supplementary Fig. 1). Taken together, our data suggest that increased neuronal activity level, induced by either artificial depolarization, physiologically relevant electrical

stimulation, or behavioral training, can lead to phosphorylation of S421 on the MeCP2 protein in the mouse hippocampus.

Recently, a detailed mass spectrometry analysis[18] identifies two serines in MeCP2 (S421 and S424), whose phosphorylation is induced by neuronal activity in the mouse brain. Yet the same study finds NAIP of MeCP2 only at S421, but not S424, in the rat brain. To completely abolish NAIP of MeCP2, we generated mice that encode serine to alanine (S to A) mutations at both the 421th and the 424th amino acids in the endogenous *Mecp2* gene[18]. The *Mecp2*$^{S421A;S424A/y}$ mice showed none of the RTT phenotypes observed in the *Mecp2* null mice (i.e. small brain or hindlimb clasping), bred normally, and had a normal lifespan ([18] and data not shown). On brain sections prepared from the *Mecp2*$^{S421A;S424A/y}$ mice, the temporal and spatial expression patterns of the MeCP2$^{S421A;S424A}$ protein were indistinguishable from those of the wild type MeCP2 protein in the wild type mice (data not shown). As an example, MeCP2$^{S421A;S424A}$ immunoreactivity (Fig. 2a) in the pyramidal neurons (co-stained by NeuN, Fig. 2b) of the CA1 region (marked by arrowheads in Fig. 2a–h) in the adult hippocampus is shown to be indistinguishable from MeCP2 immunoreactivity in the wild type (Fig. 2c,d). Moreover, the sub-cellular localization of the MeCP2$^{S421A;S424A}$ protein in cortical neurons (Supplementary Fig. 2a–d) was also identical to that of the wild type MeCP2 protein (Supplementary Fig. 2e–h). In brain lysates prepared from the *Mecp2*$^{S421A;S424A/y}$ mice, the MeCP2$^{S421A;S424A}$ protein was expressed at the same level as that of the MeCP2 protein in wild type mice both under normal condition and after seizure (Fig. 2i). We next examined the phosphorylation status of S421 in the *Mecp2*$^{S421A;S424A/y}$ and control mice. Consistent with our expectation, while phosphorylation at S421 was present at baseline (Fig. 2g,i) and greatly induced by seizure in the wild type brain (Fig. 2i), it was completely abolished in the *Mecp2*$^{S421A;S424A/y}$ mice both at baseline (Fig. 2e,i) and after seizure (Fig. 2i). By RT-PCR based sequencing of the expressed *Mecp2*$^{S421A;S424A}$ RNA transcript, we have previously shown that S424 has been changed to A424[18]. Since the mutation to alanine is a proven way to abolish serine phosphorylation, A424 cannot be phosphorylated under any conditions in the *Mecp2*$^{S421A;S424A/y}$ mice. Taken together, these results suggest that the S421A;S424A double mutation specifically abolished NAIP of MeCP2, without changing the expression level, expression pattern and intracellular localization of the mutant protein.

Enhanced hippocampal memory in *Mecp2*$^{S421A;S424A/y}$ mice

To reveal the physiological relevance of neuronal activity-induced MeCP2 phosphorylation, we performed a series of behavioral analyses of the *Mecp2*$^{S421A;S424A/y}$ mice. To eliminate potential influence of different genetic backgrounds on animal behavior, we backcrossed the *Mecp2*$^{S421A;S424A}$ mice with the C57BL/6 mice for a minimum of 10 generations. As an initial screen for phenotypes covering anxiety, exploratory activity, motor coordination, and learning and memory, we compared the *Mecp2*$^{S421A;S424A/y}$ mice to their wild type littermates in the open field test, the rotarod test, and the fear conditioning test. In the open field test, the *Mecp2*$^{S421A;S424A/y}$ mice showed a similar level of anxiety, as measured by the percentages of distance traveled in the middle and the corners of the field, as their wild type littermates (Supplementary Fig. 4a,b); and the same amount of exploratory activity, as measured by the total distance traveled, as their wild type littermates (Supplementary Fig.

4c). To confirm these results, we performed another widely used anxiety test--the elevated plus maze--with another cohort of *Mecp2*$^{S421A;S424A/y}$ mice and their wild type littermates, and observed similar levels of exploratory activity and anxiety in the *Mecp2*$^{S421A;S424A/y}$ mice and their wild type littermates (Supplementary Fig. 4d–f). In a test for motor coordination, the *Mecp2*$^{S421A;S424A/y}$ mice fell off the rotating rod slightly quicker than their wild type littermate (Supplementary Fig. 4g). However, the difference was not statistically significant ($p = 0.3$).

After the first two screening tests yielded no difference, we observed a strong phenotype in the last test of the screening--the fear conditioning test. In this classic Pavlovian conditioning preparation aimed at studying fear learning and memory (illustrated in Fig. 3a), the *Mecp2*$^{S421A;S424A/y}$ mice froze more than their wild type littermates (Fig. 3c) in the context test, while they froze the same as the wild type littermates (Fig. 3c) in the cue test. It is widely believed that performance in the context test is dependent on the function of both the hippocampus and the amygdala, while performance in the cue test is only dependent on the function of the amygdala. Thus the combination of results from the context test and the cue test strongly suggests a difference in hippocampus function between the *Mecp2*$^{S421A;S424A/y}$ and the wild type mice. To confirm the context test results, we performed context-only training (no tone played during training, as illustrated in Fig. 3b) and testing with a fresh cohort of *Mecp2*$^{S421A;S424A/y}$ mice and their wild type littermates. The *Mecp2*$^{S421A;S424A/y}$ mice again froze more than the wild type (Fig. 3d) in the context test. In both training paradigms, no significant difference in baseline freezing (pre-shock during training sessions, and pre-tone in the cue test sessions) was observed between the *Mecp2*$^{S421A;S424A/y}$ mice and their wild type littermates (Fig. 3c–d). To further confirm the involvement of the hippocampus in an independent assay, we performed the Morris water maze test (as illustrated in Fig. 4a), a well-established hippocampus-dependent spatial learning and memory test, on yet another cohort of *Mecp2*$^{S421A;S424A/y}$ mice and their wild type littermates. The hidden platform version of the water maze test was used in this experiment. Both the *Mecp2*$^{S421A;S424A/y}$ mice and their wild type littermates swam at the same speed during training and testing (Fig. 4b). Throughout the training period, both genotypes of mice learned the location of the hidden platform equally well, as indicated by the persistent decrease in time needed to find and climb onto the platform (Fig. 4c). In the probe trials, while both the *Mecp2*$^{S421A;S424A/y}$ and the wild type mice remembered where the hidden platform was placed during training by spending significantly more time in the target quadrant than the other quadrants (indicating that both genotypes remembered the location of the platform), the *Mecp2*$^{S421A;S424A}$/*y* mice spent significantly more time than the wild type littermates in the target quadrant (Fig. 4d), which clearly demonstrated that the *Mecp2*$^{S421A;S424A/y}$ mice had better spatial memory than their wild type littermates. Taken together, these results strongly suggest the *Mecp2*$^{S421A;S424A/y}$ mice have altered hippocampal function.

Enhanced LTP and synaptogenesis in *Mecp2*$^{S421A;S424A/y}$ mice

Since our behavioral analysis identified the hippocampus as one brain region whose function was altered by abolishing activity-induced MeCP2 phosphorylation, we decided to study synaptic physiology in the hippocampus of the *Mecp2*$^{S421A;S424A/y}$ mice. In this series of

experiments, we focused our analysis on two well-characterized synapses, the Schaffer collateral-CA1 synapse and the mossy fiber-CA3 synapse. In both cases, we first examined basal synaptic transmission in the *Mecp2*$^{S421A;S424A/y}$ mice and their wild type littermates. By using extracellular field potential recording, we examined the input-output curve and paired-pulse facilitation (PPF, a form of presynaptic short term plasticity). The input-output curves showed no significant difference (Supplementary Fig. 5) between the *Mecp2*$^{S421A;S424A/y}$ mice and their wild type littermates. Similarly, no difference was detected in paired-pulse facilitation (administered at six interstimulus intervals of 25, 50, 100, 200, 300, 400 and 500ms) between the *Mecp2*$^{S421A;S424A/y}$ mice and their wild type littermates (Supplementary Figs. 6 and 7). In addition, we examined frequency facilitation at the mossy fiber-CA3 synapse, and detected no difference between the *Mecp2*$^{S421A;S424A/y}$ mice and their wild type littermates (Supplementary Fig. 8). Taken together, these results suggest abolishing NAIP at S421 and S424 of the MeCP2 protein does not alter basal synaptic transmission or presynaptic short term plasticity at either the Schaffer collateral-CA1 synapses or the mossy fiber-CA3 synapses in the hippocampus.

We next examined the long term potentiation (LTP) at both the Schaffer collateral-CA1 synapse and the mossy fiber-CA3 synapses in the *Mecp2*$^{S421A;S424A/y}$ mice. In hippocampal slices prepared from both the *Mecp2*$^{S421A;S424A/y}$ mice and their wild type littermates, LTP was readily induced by two trains of 100 Hz stimulation for 1s with an intertetanus interval of 20 s in the Schaffer collateral-CA1 synapse and lasted for 3 hours (Fig. 5a,b). At the mossy fiber-CA3 synapse, LTP was induced in both genotypes by two trains of 100 Hz stimulation for 1s with an intertetanus interval of 20 s in the presence of 50 μM D-AP5 and lasted for more than 60 minutes (Fig. 6a,b). Analysis by two-way ANOVA with repeated measures revealed significantly stronger LTP in *Mecp2*$^{S421A;S424A/y}$ mice than in their wild type littermates at both the Schaffer collateral-CA1 synapse (Fig. 5c) and the mossy fiber-CA3 synapse (Fig. 6c). At the Schaffer collateral-CA1 synapse, the late phase of the LTP was affected, since the average LTP magnitudes during the last 20 minutes of recordings were significantly different between the two genotypes (Fig. 5d). These results were consistent with the enhanced hippocampus-dependent learning and memory in these mice revealed by the fear conditioning test and the Morris water maze.

We next examined whether there were any changes at the cellular level that may underlie the altered synaptic physiology and behavioral output of the hippocampus in the *Mecp2*$^{S421A;S424A/y}$ mice. Primary hippocampal and cortical neurons were isolated from postnatal day 0–1 *Mecp2*$^{S421A;S424A/y}$ and wild type littermate pups, and cultured separately for 21 days *in vitro* (DIV). Triple immunostaining of VGLUT1 (excitatory presynaptic marker), PSD95 (postsynaptic marker), and MAP2 (dendritic marker) was performed to examine the development of excitatory synapses (Fig. 7a). Quantification of the densities of VGLUT1 puncta, PSD95 puncta, and co-localized VGLUT1/PSD95 puncta was performed along MAP2 labeled neurites (Fig. 7b,d). In the hippocampal culture, our analysis revealed a 45% increase in the number of VGLUT1 puncta ($p = 0.00003$), a 28% increase in the number of PSD95 puncta ($p = 0.005$), and a 152% increase in the number of co-localized VGLUT1/PSD95 puncta ($p = 0.000002$) in *Mecp2*$^{S421A;S424A/y}$ neurons, compared to those in the wild type neurons (Fig. 7c). In the cortical culture, similar analysis revealed a 99%

increase in the number of VGLUT1 puncta (p = 0.00002), a 37% increase in the number of PSD95 puncta (p = 0.002), and a 84% increase in the number of co-localized VGLUT1/PSD95 puncta (p = 0.04) in *Mecp2*$^{S421A;S424A/y}$ neurons, compared to those in the wild type neurons (Fig. 7e). Since co-localized VGLUT1/PSD95 puncta likely represent functional excitatory synapses, our results strongly suggest an increase in excitatory synaptogenesis in both the hippocampal and cortical neurons from the *Mecp2*$^{S421A;S424A/y}$ mice. These results are consistent with the enhanced hippocampal LTP and the enhanced learning and memory phenotypes observed in these mice.

Altered gene expression in *Mecp2*$^{S421A;S424A/y}$ hippocampus

Given the well-established role of MeCP2 in modulating gene transcription[5,8], we suspected potential gene transcription changes may underline the cellular, synaptic, and behavioral phenotypes observed in the *Mecp2*$^{S421A;S424A/y}$ mice. To reveal what gene transcription changes are caused by the loss of NAIP of MeCP2 in these mice, we first examined known MeCP2 target genes with established neuronal functions. *Bdnf* is such a gene[16,20]. We microdissected the hippocampus from the *Mecp2*$^{S421A;S424A/y}$ mice (n = 14) and their wild type littermates (n = 14), extracted RNA, performed realtime PCR, and detected an increase in *Bdnf* transcript covering its protein coding region (Bdnf CDS) in the *Mecp2*$^{S421A;S424A/y}$ hippocampus (Fig. 8a). In addition, we found an increase in *Bdnf* transcript covering its neuronal specific promoter (Exon IV, Bdnf E4) in the *Mecp2*$^{S421A;S424A/y}$ hippocampus (Fig. 8a). The increase in *Bdnf* transcription is consistent with the observed phenotypes of enhanced hippocampal LTP and hippocampus-dependent learning and memory in the *Mecp2*$^{S421A;S424A/y}$ mice.

Recognizing that the phenotypes of the better contextual fear memory, the enhanced hippocampal LTP, the increased excitatory synaptogenesis, and the increase in *Bdnf* transcription in the *Mecp2*$^{S421A;S424A/y}$ mice are similar to those observed in transgenic mice overexpressing *Mecp2* (*Mecp2*^{Tg})[8,21,22], we examined the expression of three additional genes whose levels were changed in the *Mecp2*^{Tg} mice[8]. These included myocyte enhancer factor 2 (*Mef2c*), bone morphogenetic protein 4 (*Bmp4*), and metabotropic glutamate receptor 1 (*Grm1*), all of which are important for the development and function of the nervous system. Moreover, MeCP2 has been shown to directly bind to the promoter of *Mef2c* and repress its transcription[8]. We found increased expression of *Bmp4* and decreased expression of *Mef2c* and *Grm1* (Fig. 8a) in the *Mecp2*$^{S421A;S424A/y}$ hippocampus. The expression change of each of the three genes in the *Mecp2*$^{S421A;S424A/y}$ mice was very similar to that in the *Mecp2*^{Tg} mice. However, it is not immediately clear how expression changes in *Bmp4*, *Mef2c* and *Grm1* may help explain the observed phenotypes in the *Mecp2*$^{S421A;S424A/y}$ mice.

Altered promoter association by the phospho-mutant MeCP2

As a first step to understand how the loss of phosphorylation may alter gene transcription, we examined the ability of the phospho-dead form of MeCP2 to bind to gene promoters. To better quantify the promoter occupancy of the phospho-dead MeCP2 protein, we generated two novel *Mecp2* knockin alleles: the *Mecp2*$^{S421A;S424A\text{-}flag/y}$ mice expressing the MeCP2$^{S421A;S424A}$-flag protein from the endogenous *Mecp2* locus and the *Mecp2*$^{WT\text{-}flag/y}$

mice expressing the MeCP2-flag protein from the endogenous *Mecp2* locus. These unique mouse lines allowed us to take advantage of a very reliable anti-flag antibody to conduct chromatin immunoprecipitation (ChIP) experiments. Western blot analysis confirmed that both the MeCP2$^{S421A;S424A}$-flag protein and the MeCP2-flag protein were expressed at the same level as the MeCP2 protein (data not shown). Behavioral testing confirmed that the *Mecp2*$^{S421A;S424A\text{-}flag/y}$ mice had enhanced hippocampus-dependent learning and memory (Supplementary Fig. 3i) similar to that observed in the *Mecp2*$^{S421A;S424A/y}$ mice, while the *Mecp2*$^{WT\text{-}flag/y}$ mice performed similar to the *Mecp2*$^{+/y}$ mice (data not shown). These data suggest that the *Mecp2*$^{S421A;S424A\text{-}flag/y}$ mice are functionally indistinguishable from the *Mecp2*$^{S421A;S424A/y}$ mice, and that the *Mecp2*$^{WT\text{-}flag/y}$ mice are functionally indistinguishable the *Mecp2*$^{+/y}$ mice.

Because the transcriptional changes detected in Fig. 8a were from the *in vivo* hippocampus, we reasoned it would be the most appropriate to use hippocampi from the *Mecp2*$^{S421A;S424A\text{-}flag/y}$ and the *Mecp2*$^{WT\text{-}flag/y}$ mice for ChIP analysis to examine promoter occupancy of the phospho-mutant form and the wild type form of MeCP2. Results from this experiment revealed increased promoter occupancy by the MeCP2$^{S421A;S424A}$-flag protein, as compared with that by the MeCP2-flag protein, on the promoters of *Bdnf*, *Bmp4*, *Mef2c*, and *Grm1* (Fig. 8b). Thus, the loss of phosphorylation appears to enhance the binding of MeCP2 to its target gene promoters. Because MeCP2 has been shown to be capable of activating the transcription of some genes and repressing the transcription of other genes at the same time[8,9], it is possible that the increased promoter occupancy of the phospho-mutant form of MeCP2 may lead to opposite transcriptional outcomes in the phospho-mutant hippocampus. More detailed studies in the future will help reveal the mechanisms of such regulations.

Discussion

NAIP of MeCP2 has been hypothesized to be a potential mechanism for dynamically regulating its binding to methylated DNA and thus its ability to coordinate neuronal gene transcription[16–18]. Yet it is not clear what, if any, function requires such phosphorylation in the *in vivo* brain. We generated the *Mecp2*$^{S421A;S424A}$ knockin mice to abolish NAIP of MeCP2, and provide here the first genetic evidence that NAIP of MeCP2 is involved in regulating several important functions in the *in vivo* brain, including promoter occupancy, gene transcription, excitatory synaptogenesis, LTP, and learning and memory.

The wide range of phenotypes observed in the *Mecp2*$^{S421A;S424A/y}$ mice spans the molecular, cellular, synaptic, and animal behavioral levels. Although it is not easy to establish causal links across all levels, the phenotypes observed in *Mecp2*$^{S421A;S424A/y}$ mice, including the increased *Bdnf* expression, the increased excitatory synaptogenesis, the enhanced hippocampal LTP, and the enhanced hippocampus-dependent learning and memory, are very consistent with each other. Moreover, the *Mecp2*$^{S421A;S424A/y}$ mice and the *Mecp2*^{Tg} mice[8,21,22] showed remarkable phenotypic similarities across the levels of promoter occupancy, gene expression, excitatory synaptogenesis, synaptic physiology, and animal behavior, raising the possibility that these two mouse models may share some common underlying mechanisms. While these two mouse models appear to converge on the same

molecular event--increased promoter occupancy, they achieve it through different means. In the *Mecp2* phospho-mutant mice, the expression level of the phospho-mutant protein is not altered. Yet the loss of NAIP makes it bind more tightly to gene promoters. In the *Mecp2*^{Tg} mice, the increase in MeCP2 protein level resulted in enhanced binding of MeCP2 at the promoters of its target genes. Together, these studies highlight the need in precisely regulating the ability of MeCP2 to bind to gene promoters.

Previously, Zhou *et al*.[17] showed that, using a lentivirus-based approach to simultaneously knockdown endogenous MeCP2 and express exogenous MeCP2^{S421A} in cultured neurons, loss of phosphorylation at S421 led to reduced *Bdnf* transcription. Several factors may have contributed to the apparent discrepancy between this publication and our current findings. First, we abolished potential phosphorylation at both S421 and S424 by mutating both serines to alanines, while Zhou *et al*. only mutated S421. Second, our results came from the adult hippocampus of living mice, while results in Zhou *et al*. came from cultured neurons that were isolated from embryonic rat brain. Thus, not only our *in vivo* system is different from their *in vitro* system, but also the age and species of the animals used in the two studies are significantly different. Third, it is also possible that the efficiencies of knocking down the endogenous wild type MeCP2 and the viral infection may not have been 100% in Zhou *el al*, which may have resulted in either the presence of both the wild type MeCP2 and the mutant MeCP2^{S421A} in the same neuron or the mixture of wild type and mutant neurons in the same culture. Nonetheless, our finding of the elevated *Bdnf* level *in vivo* is consistent with the enhanced LTP and better spatial memory in the *Mecp2*$^{S421A;S424A/y}$ mice, which, interestingly, were also observed in the *Mecp2*^{Tg} mice.

Several important questions remain unanswered, and await more extensive studies in the future. First, the precise synaptic mechanisms linking MeCP2 phosphorylation with hippocampal LTPs remain elusive. Since it is widely believed that pre-synaptic changes underlie CA3 LTP and post-synaptic changes underlie CA1 LTP, the loss of MeCP2 phosphorylation appears to cause both pre- and post-synaptic changes. This is possible because activity-induced MeCP2 phosphorylation could happen in both pre- and post-synaptic neurons. Second, although our data of enhanced CA1 LTP in the *Mecp2*$^{S421A;S424A/y}$ mice at late time points (160–180 minutes after LTP induction) are consistent with a change in the transcription-dependent phase of LTP (late or L-LTP), no unequivocal conclusion can be drawn because no transcription inhibitors were included in our experiment. We also note that while CA1 LTP in the *Mecp2*$^{S421A;S424A/y}$ mice appears to be enhanced at early time points after LTP induction, it is not clear how MeCP2 phosphorylation may be involved in transcription-independent regulation of synaptic plasticity. Finally, because we focused our attention on revealing the functional relevance of activity-induced MeCP2 phosphorylation *in vivo*, the gene transcription and promoter occupancy analysis included here was limited to a few candidate genes. However, given that MeCP2 is capable of binding to a single methylated CpG pair[4] and is widely distributed across the genome[23], it is highly likely that altered MeCP2$^{S421A;S424A}$ occupancy may happen at other genomic loci, and that additional gene expression changes may exist and also underlie the cellular, synaptic, and behavioral phenotypes observed in the *Mecp2*$^{S421A;S424A/y}$ mice. To fully understand the molecular mechanisms underlying these

phenotypes, it is important to study in the future, where the MeCP2$^{S421A;S424A}$ protein binds the DNA across the genome, whether and how the loss of phosphorylation may affect its association with other chromatin remodeling complexes, and ultimately how neuronal gene transcription is altered by the loss of phosphorylation.

Methods

Mouse genotyping

Two PCR genotyping assays were developed. Primers for the first assay were 5′-TCACAAGTTAACAGTGCCAGCTGC-3′(forward) and 5′-ACCCCCTTGGGACTGAAGTTACAGA-3′ (reverse). A ~100 bp band in this assay represents the wild type *Mecp2* allele. A ~200 bp band in this assay represents the *Mecp2*$^{S421A;S424A}$ allele. Primers for the second assay were 5′-CGAGGAGGCGCACTGGAAGCA-3′ (forward) and 5′-ACCTGACTGTGCTTGTCGGTAAG (reverse). A 413 bp band in this assay represents the *Mecp2*$^{S421A;S424A}$ allele.

Immunostaining and Western blot analyses of S421 phosphorylation

Anti-MeCP2 (Abcam), anti-phospho-S421 (custom made by Covance), anti-tubulin (Sigma), anti-NeuN (Santa Cruz), and anti-actin (Sigma) were used. For immunostaining, 10–12 weeks old mice were transcardially perfused with normal saline solution followed by 4% paraformaldehyde (PFA). Brains were dissected, post-fixed in 4% PFA, cryoprotected in 30% sucrose, embedded and frozen in Tissue Tek. Serial coronal sections were cut at 40 μm throughout the brain, and stained with appropriate primary and secondary antibodies. For Western blot, brains were quickly dissected out from 10–12 weeks old mice and homogenized in RIPA buffer containing both the protease inhibitor cocktail (Roche) and the protein phosphatase inhibitor cocktail (Roche). Lysate was run on 10% NuPAGE Bis-Tris gel (Invitrogen), and transferred to Protran BA 85 nitrocellulose membranes (Whatman). The membrane was incubated with appropriate primary and IR dye-conjugated secondary antibodies (Thermo Scientific), and scanned by the Odyssey infrared imaging system.

Mouse behavioral tests

10–12 weeks old mice were used in all tests. All protocols were approved by the Institutional Animal Care and Use Committee at University of Wisconsin-Madison.

Open field arena—Each mouse was placed in the center of a transparent plastic chamber (41 x 41 x 30 cm) and allowed to explore freely for 15 min, while an overhead computer-controlled camera monitored its activity. Automated data analysis was done using LimeLight2 (Coulbourn Instruments, Whitehall, PA, USA).

Elevated Plus-Maze—Each mouse was placed in the center of the maze, consisting four perpendicular arms (Two enclosed by 20 cm walls; the other two open) elevated 40 cm above ground, and allowed explore freely for 10 min, while an overhead computer-controlled camera monitored its behavior. The percentage of time each mouse spent in the open arms and the closed arms was measured using the LimeLight2 sofeware.

Rotarod test—Mice were placed onto a horizontal rotating rod, with the rotation speed accelerating from 2 rpm to 20 rpm over 5 min. A test lasted from the time the mouse was placed on the rod until it fell off or until 5 min had elapsed.

Fear conditioning test—In training paradigm I, mice were placed into a shock chamber and allowed to explore for 2 min. Then, a white noise tone (87 dB) sounded for 30 sec (conditional stimulus or "CS"). During the last 1.5 sec of the tone, mice received a mild footshock (0.5 mA) (unconditioned stimulus or "US"). 2 min later, the same tone-footshock (CS-US) combination was delivered again. 1 min after the end of the second CS-US, mice were returned to their home cages. The context test was performed 22 hr after the training. During the test, mice were placed back into the same training chamber, and monitored by an overhead camera in the chamber for 5 min. 2 hr after the context test, the cue test was performed, in which colored plexiglass inserts were placed into the training chamber to hide the shock grid and to change the "context" of the chamber. Mice were then placed in the chamber and monitored by the overhead camera for 6 min, during which two CS (spaced the same way as in the training session) were given. In training paradigm II, everything stayed the same except that no tones (CS) were given. Only the context test was administered on the mice trained in training paradigm II. All events in the fear conditioning test were programmed and data recorded through the FreezeFrame2 and FreezeView software from (Actimetrics Software, Wilmette, IL, USA).

Morris water maze—Mice were trained to locate a hidden platform (1 cm below the surface of the water) in a circular pool (1.20 m in diameter) of opaque water using distal visual cues. Mice were given 2 blocks of 4 training trials a day for 4 consecutive days. During a training trial, each mouse was released into the pool from 1 of 4 starting positions in a random order. The location of the hidden platform remained constant throughout training. Time to find the platform was measured in each trial. If a mouse did not find the platform within 60 sec, it was gently guided by hand onto the platform and allowed to remain there for 10 sec. After 4 days, the probe test was performed with no platform. Each mouse was allowed to search the platform for 60 sec, while an overhead camera recorded its movement. Time spent searching in each quadrant by a mouse was used to characterize its search behavior.

Electrophysiology

8–12 weeks old mice were anesthetized and killed by decapitation. 400 μM transverse hippocampal slices were prepared using a Vibratome Tissue Chopper. Slices were recovered in oxygenated ACSF at room temperature for at least 1 hr. The ACSF contained (in mM): 124 NaCl, 2.5 KCl, 1.25 NaH_2PO_4, 26 $NaHCO_3$, 1.2 $MgCl_2$, 2.5 $CaCl_2$, and 15 glucose. All recordings were performed at 30 ± 1 °C in a submerged chamber (Warner instruments, Hamden, CT) continuously superfused with oxygenated ACSF. Schaffer collateral-CA1 synaptic responses and mossy fiber-CA3 synaptic responses were recorded as extracellular field potentials (fEPSPs) from the CA1 stratum radiatum and the CA3 stratum lucidum area, respectively. Unless otherwise-mentioned, test stimuli were delivered at a frequency of 0.05 Hz. The stimulus intensity was set to produce 25–30% of the maximum response in all the experiments. Paired-pulse facilitation (PPF) was performed at 25, 50, 100, 200, 300, 400,

and 500 ms interstimulus intervals. Frequency facilitation was investigated by increasing the stimulation rate from 0.1 Hz to 0.5 Hz. LTP was induced by two trains of 100 Hz stimulation lasting 1 s with a 20 s intertetanus interval. No bicuculline was applied during any recording. For CA3 LTP induction, tetanus was delivered in the presence of 50 mM D-(2)-2-amino-5-phosphonopentanoic acid (D-APV) to prevent contamination of the NMDA-dependent pathway converging on CA3 neurons. Mossy fiber synaptic responses were identified by large PPF and frequency facilitation. Experiments were included for data analysis only if DCG-IV caused a greater than 75% reduction in the synaptic response. For Schaffer collateral-CA1 recordings, fEPSP rise slope was calculated as the slope of the rising phase 20–80% of the peak response. For CA3 recordings, the amplitude of individual synaptic response was measured after subtraction of the response that remained in the presence of DCG-IV. Data were acquired and analyzed with pClamp10.2 software (Axon Instruments, Sunnyvale, CA). Signals were filtered at 2 Hz and sampled at 10 kHz by Digidata 1440A (Axon Instruments, Sunnyvale, CA). Traces were averaged for every 2 min interval.

Analysis of excitatory synaptogenesis in cultured hippocampal and cortical neurons

Dissociated hippocampi and cortical neurons were isolated from postnatal day 0 or day 1 *Mecp2*$^{S421A;S424A/y}$ and *Mecp2*$^{+/y}$ pups, and plated at a density of 1 x $10^4/cm^2$ on poly-L-lysine (Sigma# P2636) coated coverslips. Culture medium was Neurobasal (Invitrogen #21103-049) containing 2% B27 (Invitrogen #12587-010), 1% N2 (invitrogen#17502-048), and 0.5 mM GlutaMax (Invitrogen#35050-061). Cultured hippocampal and cortical neurons were fixed at DIV (days in vitro) 21 with 4% PFA and 4% sucrose in PBS, washed with PBS, permeabilized with Tritonx-100 in PBS, blocked with 10% Normal Donkey Serum in PBS (all at room temperature), and incubated at 4 °C overnight with mouse anti-MAP2 (Millipore#05-346, 1:300), rabbit anti-PSD95 (Cell Signaling#2507, 1:200) and goat anti-VGLUT1 (Santa Cruz#sc-13320, 1:200) antibodies in PBS containing 10% normal donkey serum. The next day, after being washed in PBS, the coverslips were incubated with secondary antibodies, including AffiniPure F(ab′)$_2$ Fragment donkey IgG(H+L) conjugated with DyLight-488 (anti-goat),-549 (anti-rabbit), -649 (anti-mouse) respectively (1:200, Jackson immunoResearch Laboratories). Coverslips were then washed in PBS and stained with DAPI before being mounted on glass slides with FLUOROMOUNT G (SouthernBiotech#0100-01).

Image analysis

Images in Figures. 1 and 7 were captured on a Nikon A1RSI confocal microscope. For each experimental series, all the images were acquired with identical settings for laser power, photomultiplier gain and offset. Z-stacks were collapsed in a maxmum projection and analyzed with NIH ImageJ software. For quantification of MeCP2 pS421 level in CA1, all the images were quantified using a single threshold value, which is determined by the background level of the control sections in each experiment. MeCP2 pS421 level was measured as the average MeCP2 p421 intensity in the CA1 neuronal nucleus, which is identified by NeuN immunoreactivity. For pre- and post-synaptic puncta quantification of the primary neuronal cell culture, only primary dendritic branches were included in the analysis. VGLUT1 and PSD95 images were thresholded using constant settings for each

experiment, and converted to binary images. Thresholds were chosen such that all recognizable punctate structures were included into the analysis. VGLUT1 and PSD95 puncta were identified by the "partial analysis" function in ImageJ, with the minimal size 0.2 μm^2 for VGLUT1 and 0.1 μm^2 for PSD95. VGLUT1 puncta with overlap or directly adjacent PSD95 puncta were scored as colocalized VGLUT1/PSD-95 puncta. Puncta density was measured as the puncta number per μm of dendritic branch.

RNA extraction, reverse transcription, and real time PCR

Total RNA from mouse hippocampus was isolated using SV Total RNA Isolation System (Promega). cDNA was made using qScript^{TM} cDNA SuperMix (Quanta Bioscience). Real-time PCR was performed on an iQ5 Real-Time PCR machine using iQ SYBR Green Supermix (Bio-Rad). Fold change was calculated with the $2^{-\text{delta Ct}}$ method after normalization to *Gapdh*. Primers were: 5′-AATGGGAAGCTTGTCATCAACG-3′ (Gapdh-F), 5′-GAAGACACCAGTAGACTCCACGACATA-3′ (Gapdh-R), 5′-CGCCATGCAATTTCCACTATCAATAATTTAAC-3′(Bdnf E4-F), 5′-CTTTTTCAGTCACTACTTGTCAAAGTAAAC-3′ (Bdnf E4-R), 5′-GACCATCCTTTTCCTTACTATGG-3′ (Bndf CDS-F), 5′-CCATTCACGCTCTCCAGAGTC-3′ (Bdnf CDS-R), 5′-CATCACGAAGAACATCTGGAG-3′ (Bmp4-F), 5′-CGAGGAGATCACCTCATTCTC-3′ (Bmp4-R), 5′-CAACAACATATGGTACTGAGTAC-3′ (Mef2c-F), 5′-CATGTTATGTAGGTGCTGCTGC-3′ (Mef2c-R), 5′-ACAGAAGGGAATTACGGCGAGA-3′ (Grm1-F), 5′-ATCAAAGCTCTTCTCGCCAGCA-3′ (Grm1-R).

Chromatin immunoprecipitation and gene promoter specific real time PCR

Hippocampi were dissected from 9–12 weeks old mice, diced into small pieces and crosslinked in 0.5% formaldehyde, washed with ice-cold PBS, sonicated with Misonix Sonicator 3000 in lysis buffer (1% SDS, 10 mM EDTA, 20 mM Tris-HCl, pH 8.1, Roche protease inhibitor cocktail), and cleared by centrifugation to generate sheared chromatin. Dynabeads (Invitrogen) were pre-washed with PBS/BSA (0.5% BSA in PBS) and incubated with anti-FLAG antibody (Sigma) to form the beads/antibody complex. For immunoprecipitation, sheared chromatin was diluted in dilution buffer (0.01% SDS, 1.1% Triton X-100, 1.2 mM EDTA, 16.7 mM Tris-HCl, pH 8.1, 167 mM NaCl) and incubated with beads/antibody complex overnight on a Nutator at 4 oC. The next day, the beads/antibody/chromatin complex were washed with washing buffer (50 mM Hepes, pH 7.6, 1 mM EDTA, 0.7% DOC, 1% NP-40, 0.5 M LiCl) and TBS. The immunoprecipitated chromatin was then eluted from the beads in elution buffer (1% SDS, 10 mM EDTA, 20 mM Tris-HCl, pH 8.1), and reverse-crosslinked. Sheared chromatin not incubated with beads/antibody complex was processed the same way to generate input DNA. Both ChIP DNA and input DNA were treated with RNase A (Thermo Scientific) and proteinase K (Promega), purified by ethanol precipitation, and dissolved in water (Promega). 20 ng of ChIP DNA and input DNA was used for each quantitative real-time PCR. Real-time PCR was performed on an iQ5 Real-Time PCR machine using iQ SYBR Green Supermix (Bio-Rad). The ChIP DNA level was normalized to the input DNA level using the $2^{-\text{delta Ct}}$ method. Relative promoter occupancy was calculated by setting the MeCP2-flag binding

level as 100%. Primers were: 5′-TTCTGTGTGCGTGAATTTGC-3′ (Bdnf E4-F), 5′-TGGGTGGGAGTCCACGAG-3′ (Bdnf E4-R), 5′-TACAGTAGCATTGTGGGTTC-3′ (Mef2c-F), 5′-AGGAGGGATTAATCATGCTC-3′ (Mef2c-R), 5′-CTCTAGTGTTTTCATGTGAC-3′ (Grm1-F), 5′-GGAGTAGCCAAATGTAGAGT-3′ (Grm1-R), 5′-TGAAGCTGATAGTTCCTTCC-3′ (Bmp4-F), 5′-GCTAGCTGGGAGGTGGAATG-3′ (Bmp4-R).

Statistical analysis

For Morris water maze data, two way ANOVA with repeated measures was performed to reveal any significant interaction between genotype and quadrant, which was followed by a Tukey-HSD *post hoc* test to complete the pairwise comparison of the percentage of time spent by each genotype in each quadrant. For LTP and basic synaptic transmission data, two-way ANOVA with repeated measures was performed. For the rest of the data, the Student's t-test was performed. Statistical significance was determined at $p < 0.05$.

Supplementary Material

Refer to Web version on PubMed Central for supplementary material.

Acknowledgments

We thank Drs. Albee Messing, John Svaren, and Jerry Yin for critically reading the manuscript, Shruti Marwaha for assistance with mouse work, and Dr. Matthew Andrzejewski for assistance with statistical analysis. H.L. was supported by a pre-doctoral fellowship from the Stem Cell and Regenerative Medicine Center at the University of Wisconsin-Madison. E.C.W. was supported by a predoctoral training grant (5T32GM07133) and a graduate student fellowship from the Friends of the Waisman Center. Q.C. was supported by a Young Investigator Award from NARSAD. This work was partially supported by grants from NICHD (R01 HD064743 and R21 HD066560 to Q.C. and P30 HD03352 to the Waisman Center).

References

1. Miller CA, Sweatt JD. Covalent modification of DNA regulates memory formation. Neuron. 2007; 53:857–69. [PubMed: 17359920]
2. Miller CA, et al. Cortical DNA methylation maintains remote memory. Nat Neurosci. 13:664–6. [PubMed: 20495557]
3. Feng J, et al. Dnmt1 and Dnmt3a maintain DNA methylation and regulate synaptic function in adult forebrain neurons. Nat Neurosci. 13:423–30. [PubMed: 20228804]
4. Lewis JD, et al. Purification, sequence, and cellular localization of a novel chromosomal protein that binds to methylated DNA. Cell. 1992; 69:905–14. [PubMed: 1606614]
5. Nan X, Campoy FJ, Bird A. MeCP2 is a transcriptional repressor with abundant binding sites in genomic chromatin. Cell. 1997; 88:471–81. [PubMed: 9038338]
6. Jones PL, et al. Methylated DNA and MeCP2 recruit histone deacetylase to repress transcription. Nat Genet. 1998; 19:187–91. [PubMed: 9620779]
7. Bird AP, Wolffe AP. Methylation-induced repression--belts, braces, and chromatin. Cell. 1999; 99:451–4. [PubMed: 10589672]
8. Chahrour M, et al. MeCP2, a key contributor to neurological disease, activates and represses transcription. Science. 2008; 320:1224–9. [PubMed: 18511691]
9. Yasui DH, et al. Integrated epigenomic analyses of neuronal MeCP2 reveal a role for long-range interaction with active genes. Proc Natl Acad Sci U S A. 2007; 104:19416–21. [PubMed: 18042715]

10. Amir RE, et al. Rett syndrome is caused by mutations in X-linked MECP2, encoding methyl-CpG-binding protein 2. Nat Genet. 1999; 23:185–8. [PubMed: 10508514]
11. Van den Veyver IB, Zoghbi HY. Methyl-CpG-binding protein 2 mutations in Rett syndrome. Curr Opin Genet Dev. 2000; 10:275–9. [PubMed: 10826991]
12. Wan M, et al. Rett syndrome and beyond: recurrent spontaneous and familial MECP2 mutations at CpG hotspots. Am J Hum Genet. 1999; 65:1520–9. [PubMed: 10577905]
13. Xiang F, et al. Mutation screening in Rett syndrome patients. J Med Genet. 2000; 37:250–5. [PubMed: 10745042]
14. Hagberg B. Rett's syndrome: prevalence and impact on progressive severe mental retardation in girls. Acta Paediatr Scand. 1985; 74:405–8. [PubMed: 4003065]
15. Hagberg B, Hagberg G. Rett syndrome: epidemiology and geographical variability. Eur Child Adolesc Psychiatry. 1997; 6 (Suppl 1):5–7. [PubMed: 9452911]
16. Chen WG, et al. Derepression of BDNF transcription involves calcium-dependent phosphorylation of MeCP2. Science. 2003; 302:885–9. [PubMed: 14593183]
17. Zhou Z, et al. Brain-specific phosphorylation of MeCP2 regulates activity-dependent Bdnf transcription, dendritic growth, and spine maturation. Neuron. 2006; 52:255–69. [PubMed: 17046689]
18. Tao J, et al. Phosphorylation of MeCP2 at Serine 80 regulates its chromatin association and neurological function. Proc Natl Acad Sci U S A. 2009; 106:4882–7. [PubMed: 19225110]
19. Deng JV, et al. MeCP2 in the nucleus accumbens contributes to neural and behavioral responses to psychostimulants. Nat Neurosci.
20. Martinowich K, et al. DNA methylation-related chromatin remodeling in activity-dependent BDNF gene regulation. Science. 2003; 302:890–3. [PubMed: 14593184]
21. Collins AL, et al. Mild overexpression of MeCP2 causes a progressive neurological disorder in mice. Hum Mol Genet. 2004; 13:2679–89. [PubMed: 15351775]
22. Chao HT, Zoghbi HY, Rosenmund C. MeCP2 controls excitatory synaptic strength by regulating glutamatergic synapse number. Neuron. 2007; 56:58–65. [PubMed: 17920015]
23. Skene PJ, et al. Neuronal MeCP2 is expressed at near histone-octamer levels and globally alters the chromatin state. Mol Cell. 37:457–68. [PubMed: 20188665]

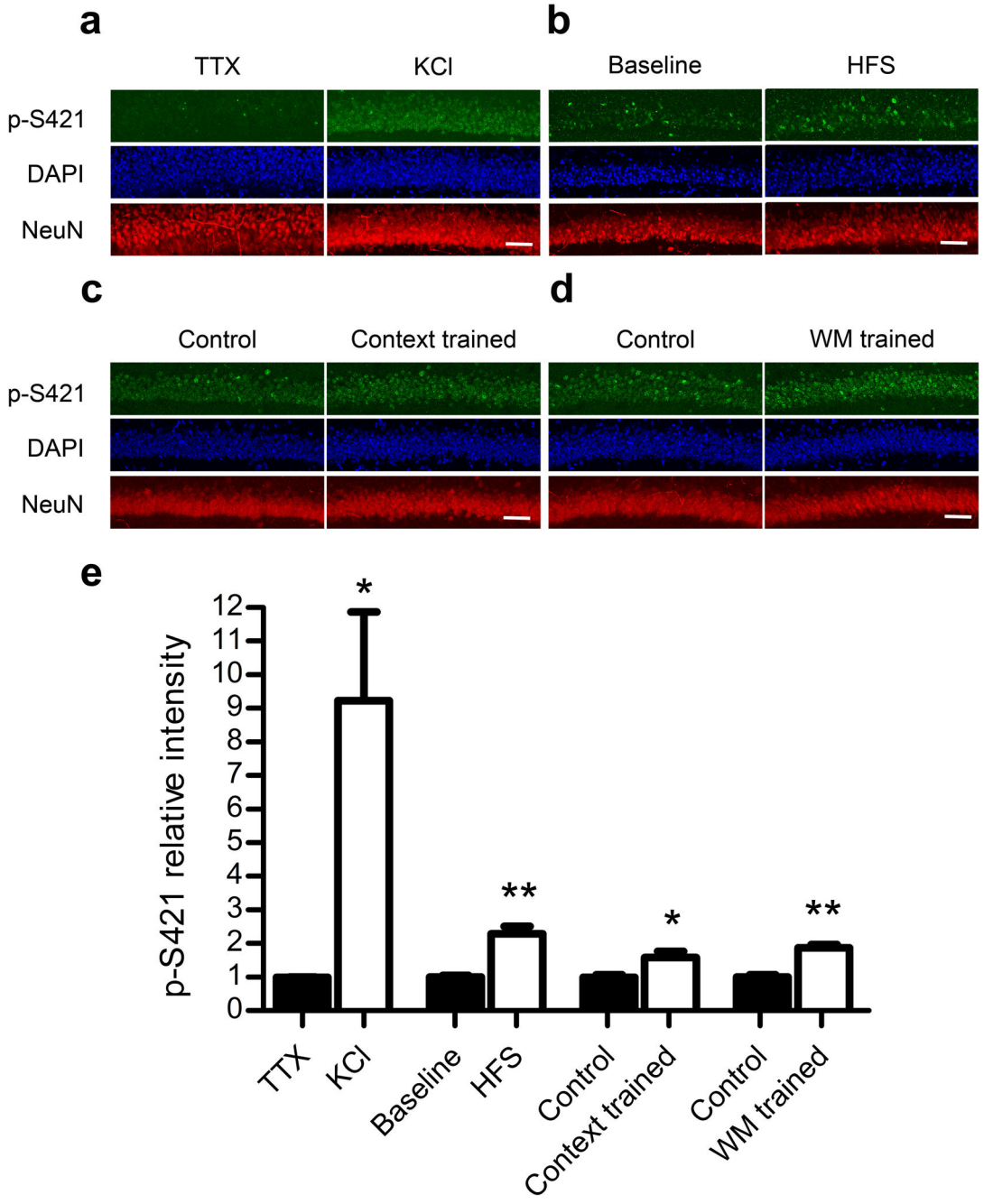

Figure 1.

Phosphorylation at serine 421 induced by depolarization, high frequency stimulation and behavioral trainings. (a–d) Representative confocal microscope images of co-staining of DAPI (labeling all cell nuclei), NeuN (labeling all neuronal nuclei), and p-S421 in the CA1 region of hippocampal slices treated with 1 μM TTX or 50 mM KCl for one hour (a), receiving baseline stimulation or high frequency stimulation (HFS, 100 Hz, 1 s, twice with 20 s interval) (b), from mice that received shock immediately after being put into the box (immediate shock control) and mice that received shock two minutes after being put into the

box (context trained) (c), or from mice that received the hidden platform version of Morris water maze (WM) training (WM trained) and mice that swam the same amount of time in the same tank with no platform (yoked/swimming control) (d). Scale bars = 20 μm. (e) Quantification of relative p-S421 intensity in the depolarization experiment (n = 4 for each group), high frequency stimulation experiment (n = 4 for each group), the contextual fear training experiment (n = 5 for each group), and the Morris water maze training experiment (n = 3 for each group). Data are presented as mean ± s.e.m. *P < 0.05. **P < 0.01.

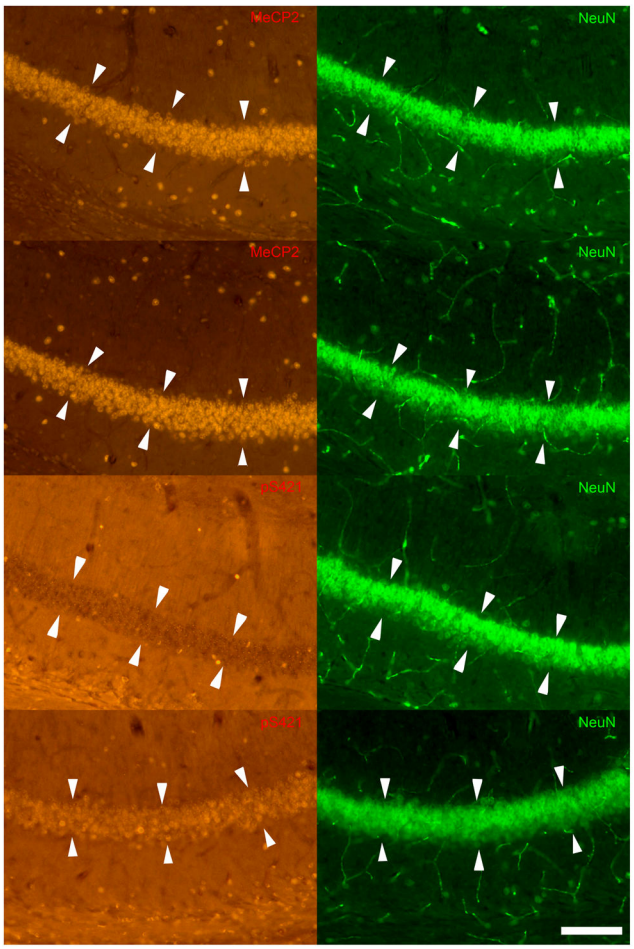

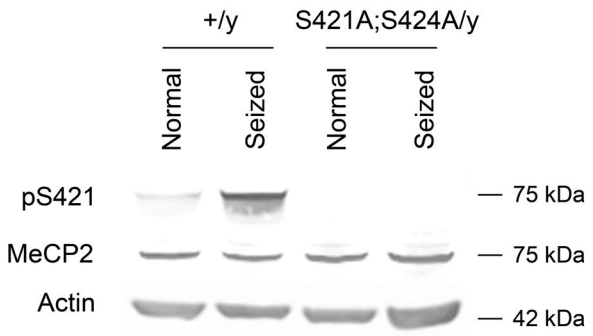

Figure 2.

Loss of NAIP at serine 421 (S421) in the *Mecp2*$^{S421A;S424A/y}$ mice.

Representative images of the CA1 region of the hippocampus from the *Mecp2*$^{S421A;S424A/y}$ mice (a, b, e, f) and their wild type littermates (c, d, g, h) co-stained with MeCP2 (a, c) and NeuN (b, d) or p-S421 (e, g) and NeuN (f, h). a and b, c and d, e and f, g and h are the red and green channels of the same images. Arrowheads in a–h mark the pyramidal cell layer in the CA1. Scale bar = 100 μm. Scale bar in h applies to a–h. (i) Western blot analysis was performed to compare the expression levels of p-S421 (top panel), MeCP2 (middle panel),

and actin (bottom panel) in the brains of the wild type (left two lanes) and *Mecp2*$^{S421A;S424A/y}$ mice (right two lanes) under normal condition and after seizure. Shown here are partial blots covering the region around the expected molecular weights of the proteins of interest. Full length blots are shown in Supplementary Figure 3.

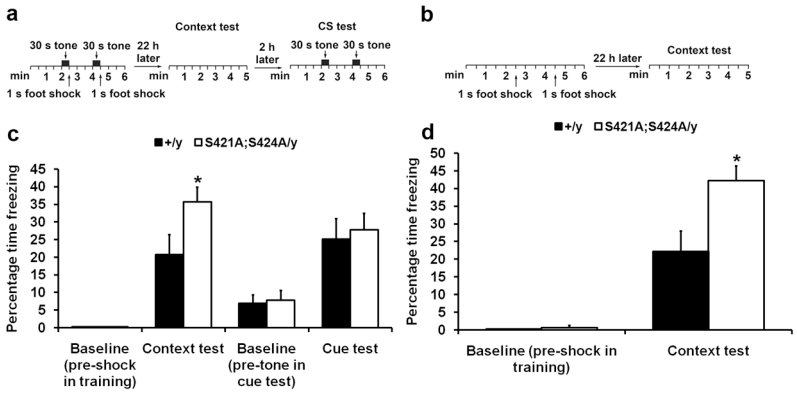

Figure 3.

Enhanced contextual fear memory in the *Mecp2*$^{S421A;S424A/y}$ mice. (a) Schematic drawing of the design of training paradigm I (tone paired with shock) and the ensuing context test and cue test. (b) Schematic drawing of the design of training paradigm II (shock only) and the ensuing context test. (c) The contextual memory and the cue memory were measured by the percentage of time the mice spent freezing 22 and 24 hours, respectively, after training. Because none of the wild type and mutant mice froze pre-shock in training sessions in training paradigm I, those bars are 0s. n = 10 in each genotype. Bar graph shows mean ± s.e.m. (d) The contextual memory was measure by the percentage of time the mice spent freezing 22 hours after training. Because none of the wild type mice froze pre-shock in training sessions in training paradigm II, that bar is 0. n = 5 in each genotype. Bar graph shows mean ± s.e.m. *P < 0.05.

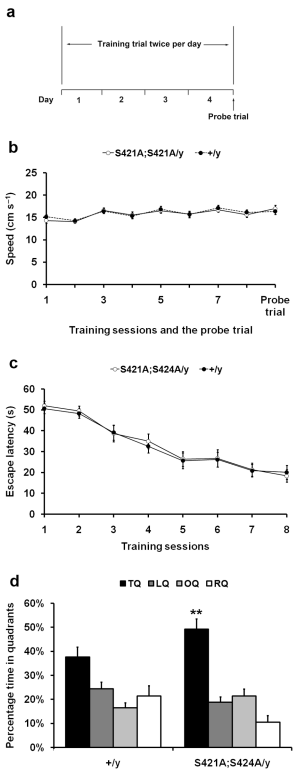

Figure 4.

Enhanced spatial memory in the *Mecp2*$^{S421A;S424A/y}$ mice. (a) Schematic drawing of the Morris water maze test design. (b) Swimming speeds of the wild type and the *Mecp2*$^{S421A;S424A/y}$ mice measured during the training sessions and probe trials. (c) Escape latency (time to find the hidden platform) plotted against the 8 training sessions over 4 days. (d) Percentage of time spent in the target quadrant (TQ), the quadrant left to the TQ (LQ), the quadrant opposite to the TQ (OQ), and the quadrant right to the TQ (RQ) during the probe trial. n = 20 in each genotype. Bar graph shows mean ± s.e.m. Statistical analysis was performed as the following. First, a two way repeated measures ANOVA (One Factor Repetition) was performed, which revealed a statistically significant interaction between genotype and quadrant ($F(3,114) = 3.77$, $p = 0.01$). Subsequently, a Tukey-HSD *post hoc* test was performed on that interaction to complete the pairwise comparison of the percentage of time spent by each genotype in each quadrant, which revealed that both the wild type and the *Mecp2*$^{S421A;S424A/y}$ mice spent significantly more time in the target quadrant (in which a hidden platform was placed during the training sessions) than the other quadrants during the probe trial; and that most importantly, the *Mecp2*$^{S421A;S424A/y}$ mice spent significantly more time in the target quadrant than their wild type littermates did (49% vs. 37%, $p = 0.01$). **$P < 0.01$.

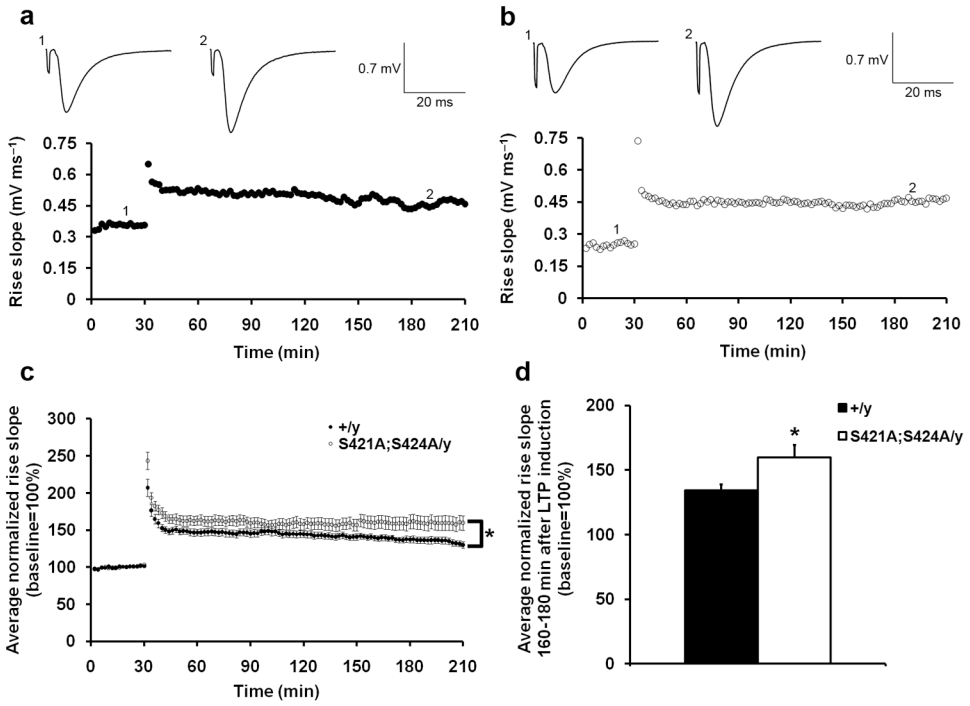

Figure 5.

Enhanced Schaffer collateral-CA1 LTP in the *Mecp2*$^{S421A;S424A/y}$ mice. (a,b) Representative recording of field EPSP (fEPSP) rise slope in wild type (a) and the *Mecp2*$^{S421A;S424A/y}$ (b) slices. Sample traces in each genotype represent before (1) and 160 minutes after (2) the tetanic stimulation (100 Hz, 1 s, twice with 20 s interval). (c) Average normalized (against baseline) fEPSP rise slope in the wild type (closed circle) and the *Mecp2*$^{S421A;S424A/y}$ (open circle) slices. Error bars represent s.e.m. Statistical analysis was done using two-way ANOVA with repeated measure. $F(1,30) = 4.67$, $p = 0.04$. (d) Average normalized (against baseline) fEPSP rise slope 160–180 minutes after the LTP induction in the wild type and the *Mecp2*$^{S421A;S424A/y}$ slices. Bar graph shows mean ± s.e.m. 16 slices from 14 *Mecp2*$^{S421A;S424A/y}$ mice and 16 slices from 15 wild type littermates were included in (c) and (d). *P < 0.05.

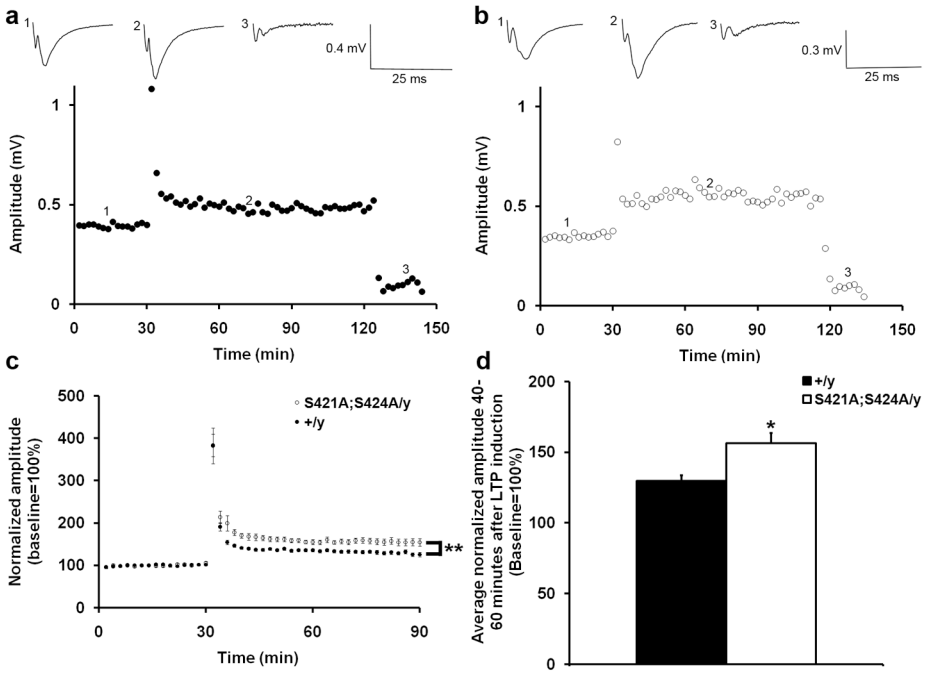

Figure 6.

Enhanced mossy fiber-CA3 LTP in the *Mecp2*$^{S421A;S424A/y}$ mice. (a,b) Representative recording of field EPSP (fEPSP) amplitudes in wild type (a) and the *Mecp2*$^{S421A;S424A/y}$ (b) slices. Sample traces in each genotype represent before (1) and 40 minutes after (2) the tetanic stimulation (100 Hz, 1 s, twice with 20 s interval), and after the application of DCG-IV (3). (c) Average normalized (against baseline) amplitudes in the wild type (closed circle) and the *Mecp2*$^{S421A;S424A/y}$ (open circle) slices. Error bars represent s.e.m. Statistical analysis was done using two-way ANOVA with repeated measure. $F(1,32) = 11.203$, $p = 0.002$. (d) Average normalized (against baseline) amplitudes 40–60 minutes after the LTP induction in the wild type and the *Mecp2*$^{S421A;S424A/y}$ slices. Bar graph shows mean ± s.e.m. 18 slices from 12 *Mecp2*$^{S421A;S424A/y}$ mice and 16 slices from 11 wild type littermates were included in (c) and (d). *$P < 0.05$. **$P < 0.01$.

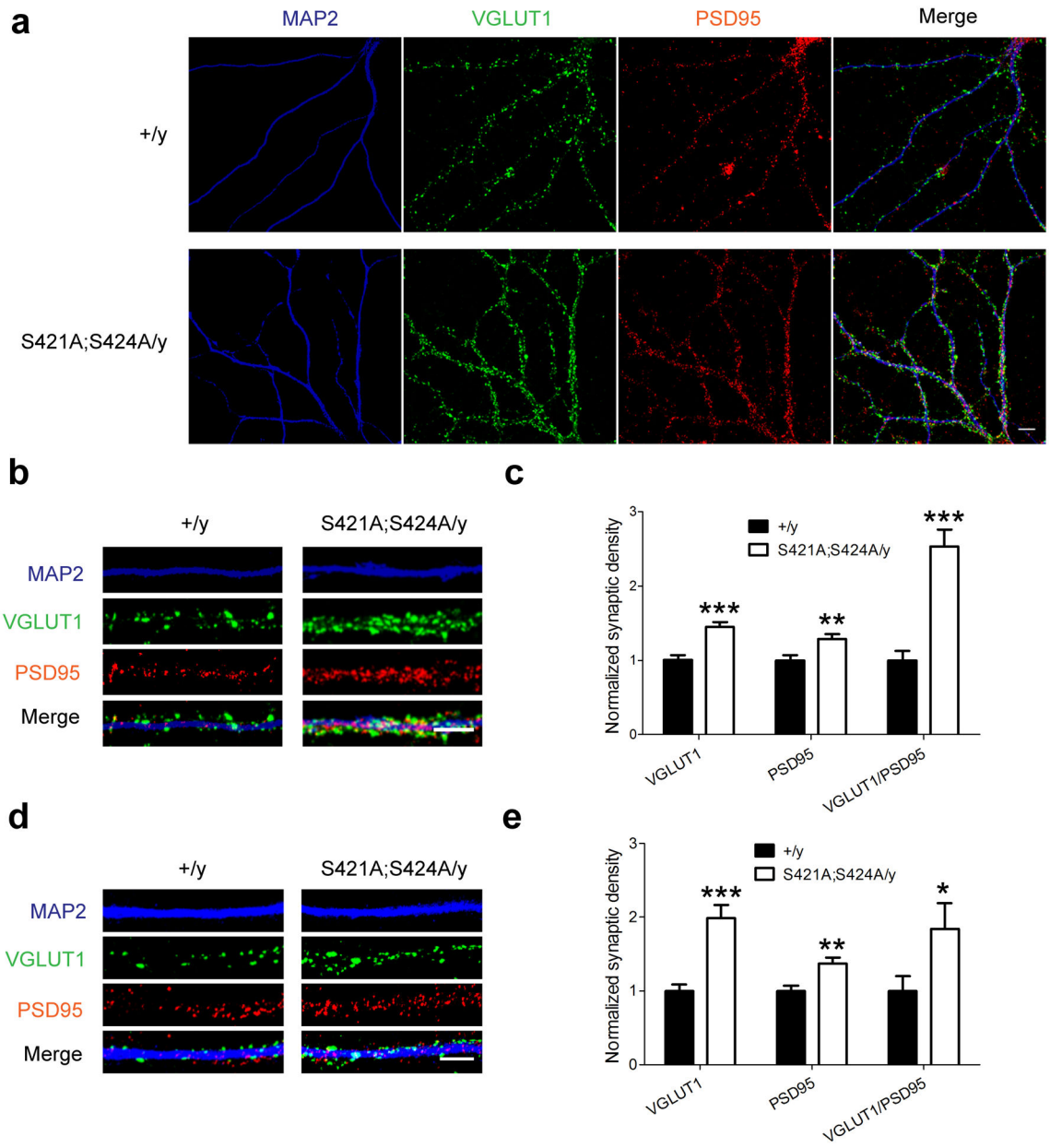

Figure 7.

Increased excitatory synaptogenesis in the *Mecp2*$^{S421A;S424A/y}$ mice. (a) Representative confocal microscope images of cultured hippocampal neurons (21 DIV) from either the *Mecp2*$^{S421A;S424A/y}$ mice or their wild type littermates co-stained with anti-VGLUT1, anti-PSD95, and anti-MAP2 antibodies. Scale bars = 10 μm. Representative images of neurites from both genotypes that were analyzed in the hippocampal culture (b) and the cortical culture (d). Quantification of the densities (number of puncta per μm) of VGLUT1 puncta, PSD95 puncta, and co-localized VGLT1/PSD95 puncta in the hippocampal culture (n = 10 in each genotype) (c) and the cortical culture (n = 12 in each genotype) (e). Numbers from the *Mecp2*$^{S421A;S424A/y}$ neurons were normalized against those from the wild type neurons. *P < 0.05. **P < 0.01. ***P < 0.001.

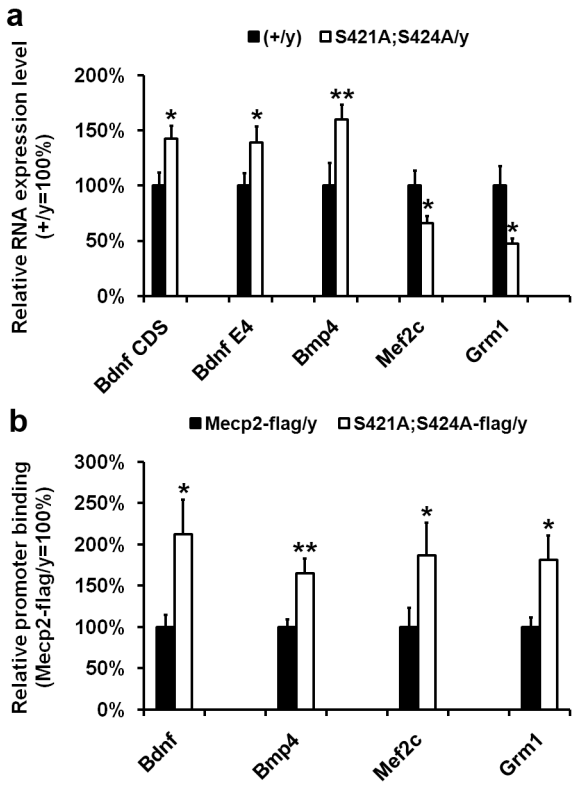

Figure 8.

Altered expression of MeCP2 target genes in the hippocampus of the *Mecp2*$^{S421A;S424A/y}$ mice and increased promoter binding by the MeCP2$^{S421A;S424A}$-flag protein. (a) Relative expression levels of *Bdnf* CDS, *Bdnf* E4, *Bmp4*, *Mef2c*, and *Grm1* in the adult hippocampus of the wild type (closed bar) and the *Mecp2*$^{S421A;S424A/y}$ mice (open bar). n = 14 in each genotype for *Bdnf* CDS, *Bdnf* E4. n = 8 in each genotype for *Bmp4*, *Mef2c*, and *Grm1*. p = 0.02 for *Bdnf* CDS. p = 0.04 for *Bdnf* E4. p = 0.01 for *Bmp4*. p = 0.05 for *Mef2c*. p = 0.02 for *Grm1*. (b) Relative binding of the MeCP2-flag and MeCP2$^{S421A;S424A}$-flag protein to the promoters of *Bdnf* (exon IV), *Bmp4*, *Mef2c*, and *Grm1* in the adult hippocampus of the *Mecp2*$^{WT\text{-}flag/y}$ mice (closed bar) and the *Mecp2*$^{S421A;S424A\text{-}flag/y}$ mice (open bar), respectively. n = 6 in each genotype. p = 0.03 for *Bdnf*. p = 0.01 for *Bmp4*. p = 0.05 for *Mef2c*. p = 0.04 for *Grm1*. *P < 0.05. **P < 0.01.